Available online at www.sciencedirect.com
SCIENCE DIRECT®
Polymer 45 (2004) 905–918
polymer
www.elsevier.com/locate/polymer

Structural formation of amorphous poly(ethylene terephthalate) during uniaxial deformation above glass temperature

Daisuke Kawakami[a], Benjamin S. Hsiao[a,*], Shaofeng Ran[a], Christian Burger[a], Bruce Fu[a], Igors Sics[a], Benjamin Chu[a], Takeshi Kikutani[b]

[a]*Department of Chemistry, State University of New York at Stony Brook, Stony Brook, NY 11794-3400, USA*
[b]*Department of Organic and Polymeric Materials, Tokyo Institute of Technology, O-okayama, Meguro-ku, Tokyo 152, Japan*

Received 27 August 2003; received in revised form 11 November 2003; accepted 14 November 2003

Abstract

An in situ study of structural formation of amorphous poly(ethylene terephthalate) (PET) during uniaxial deformation above its T_g (at 90 °C) was carried out by wide-angle X-ray diffraction (WAXD) with synchrotron radiations. Results indicate that the relationships between structure and mechanical property can be divided into three zones: I, II and III. In Zone I, oriented mesophase is induced by strain, where the applied load remains about constant but the amount of mesophase increases with strain. In Zone II, crystallization is initiated from the mesophase through nucleation and growth, where the load starts to increase marking the beginning of the strain-hardening region. The initial crystallites are defective but they form an effective three-dimensional network to enhance the mechanical property. The perfection of the crystal structure and the orientation of the crystals all increase with strain in this zone. In Zone III, the ratio between load and strain is about constant, while the stable crystal growth process takes place until the breaking of the sample. The sample damage is probably dominated by the chain pull-out mechanism from the crystal amorphous interface. The increase in molecular weight was found to enhance the overall mechanical properties such as the load to induce the mesophase and the ultimate tensile strength before breakage.

Keywords: PET; Strain-induced crystallization; Mesophase

1. Introduction

Poly(ethylene terephthalate) (PET) is one of the most widely used thermoplastic polyesters. Its most significant applications lie in the form of fibers and films. The production of PET films usually involves multiple-staged processes. In one scenario, the deformed PET melt is rapidly quenched below the glass transition temperature (T_g) and solidified into the amorphous state. The subsequent drawing processes of amorphous PET films can be carried out either below or above T_g, resulting in very different structure, morphology and properties. In our laboratory, we are particularly interested in understanding the effects of different processing conditions and material variables on the development of structure and morphology from quenched amorphous PET films. The processing conditions involve high temperature drawing above and below T_g, uniaxial and multi-axial deformation, as well as varying deformation rates. The material variables involve different molecular compositions in copolymer and polymer blends, molecular weights and distributions, as well as inclusion of nanofillers.

The structural development through the pathway of mesophase formation by the deformation of amorphous PET films below T_g has been studied quite extensively (most studies were carried out at room temperature). For example, Bonart was the first scientist who reported the structure changes during uniaxial stretching of amorphous PET, first forming a nematic phase and then a smectic phase [1]. Yeh and Geil pointed out that the strain-induced crystallization could be explained by rotation, alignment, and perfection of the internal order of the granule-like structure [2–6]. Asano et al. investigated the mesomorphic structural changes during the annealing of cold-drawn amorphous PET films and determined the mechanical properties by micro-indentation techniques [7]. They also described the transition from the nematic phase to the triclinic crystalline structure during the annealing process.

Deformation studies of amorphous PET above T_g were

* Corresponding author. Tel.: +1-631-632-7793; fax: +1-631-632-6518.
E-mail address: bhsiao@notes.cc.sunysb.edu (B.S. Hsiao).

0032-3861/$ - see front matter © 2003 Elsevier Ltd. All rights reserved.
doi:10.1016/j.polymer.2003.11.027

relatively rare probably because of the experimental difficulty at high temperatures [8–12]. The typical study dealing with this subject was usually carried out in two steps: (1) deformation at high temperatures and (2) subsequent quenching to preserve the structures in deformed samples for characterization (we term this the step-quenching technique). Using this technique, Salem studied the relationship between the structure formation and property development in deformed PET (above T_g), where he divided the process into two stages: (1) the initial stage where stress increases rapidly due to fast crystallization; and (2) the second stage where the dramatic increase in stress (strain-hardening) with only a moderate increase in crystallinity can be seen [8]. Gorlier et al. also investigated the deformation of an amorphous PET film above T_g by the step-quenching technique, but they categorized the relationships between the structural formation and the property development into three stages [9]. In the first stage, molecular orientation occurs due to strong molecular interactions. In the second stage, nuclei appear as a result of molecular orientation. At a given level of strain, the number of nuclei is fixed, forming a network structure that is responsible for strain hardening. In the last stage, crystallization develops through the growth process.

Recently, strong synchrotron X-rays made it possible to measure the structural formation in PET films and fibers during deformation in real time. Windle and coworkers studied the formation of a transient smectic phase in the fiber of random PET and PEN (polyethylene naphthalene-2,6-dicarboxylate) copolymers [13] during deformation. Blundell and coworkers also investigated the structural development of PET films during fast-drawing [14]. They reported that PET did not exhibit crystallization under fast drawing instead, a mesomorphic structure (smectic A) appears upon extension. They proposed that the smectic structure is a precursor of crystalline based on the simultaneous appearance of the triclinic crystalline peak and disappearance of the smectic peak. Unfortunately, as their experiment did not include the mechanical responses, the correlation between the structural formation and mechanical property under uniaxial deformation cannot be made. Recently, Chaari et al. [15] also reported the in situ WAXD results of PET during deformation above T_g in combination with the stress–strain curve. Unfortunately, no detailed molecular information was extracted from the WAXD data.

In our laboratory, we have previously studied in situ synchrotron X-ray measurements of an amorphous PET film during deformation below T_g (at 50 °C) and a subsequent crystallization study of the deformed sample under a constant strain at different temperatures [16]. Our results confirmed that the mesophase developed immediately upon the neck formation. As the mesophase contained a sharp meridional peak $001'$ ($d = 10.32$ Å), which was smaller than the monomer length in the typical triclinic unit cell ($c = 10.75$ Å), we concluded that the chains in the mesophase formed an inclined smectic C structure. The isotropic fraction in the diffraction pattern was separated from the anisotropic contribution using a 2D analytical technique. We further observed that both isotropic and anisotropic fractions remained about constant during crystallization under the constant strain at different temperatures. This indicated that strain-induced crystallization occurs mainly in the mesophase region.

In this study, we have continued the in situ deformation study of amorphous PET above T_g. This is because there are still some inconsistencies in the current understanding of the subject, in particular, the roles of the mesophase in the initial stages of crystallization. In addition, we have paid special attention to compare our in situ results with those from the step-quenching studies [8–12]. We are concerned that during the step-quenching processes, some additional changes in structure and morphology are inevitable; therefore, the existing literature data may not reflect the true state of structure during deformation. Finally, PET samples with two different molecular weights were chosen in this study in order to understand the effect of chain lengths (or relaxation times) on the mechanism and kinetics of strain-induced crystallization in PET above its T_g.

2. Experimental

2.1. Synchrotron measurements

Synchrotron X-ray measurements were carried out at the X3A2 beamline in the National Synchrotron Light Source (NSLS), Brookhaven National Laboratory (BNL). The wavelength of this beam line was 1.54 Å. A 3-pinhole collimator system was used to reduce the beam size to 0.6 mm in diameter [17]. A modified Instron 4410 tensile testing instrument was used in the stretching study. The modification to the tensile instrument included the mode of symmetrical stretching, which assured that the focused X-ray beam always illuminated the same position of the sample during deformation. The chosen deformation rate was 5 mm/min (i.e. 20% strain/min), and the experiment was carried out at the temperature of 90 °C. Two-dimensional (2D) WAXD patterns were accumulated over the collection period of 20 s per image using the CCD X-ray detector (MAR USA) during deformation. The sample to detector distance was 114.1 mm. The diffraction angle was calibrated by using a polypropylene standard and by an Al_2O_3 standard from the National Institute of Standards and Technology (NIST).

2.2. Sample preparation

Two PET samples were used in this study. They were experimental materials prepared by Toray Co. Ltd in Japan. The weight average molecular weights (M_w) of these samples were 35,000 and 20,000 g/mol, respectively. The

polydispersity (M_w/M_n) of the two samples was about the same (~2.0). Minimum amounts of antimony (the catalysis for polymerization) and phosphate (the additive to enhance the heat durability) were used to prepare these samples. Thus, the samples could be viewed as pure polymers that would not decompose under high molding temperatures. No other additive for copolymerization or plasticization was added. Both PET samples were dried under vacuum at 150 °C for 6 h after crystallization at 120 °C for 3 h in air. They were molded into a dumbbell-shape at 270 °C followed by rapid quenching with ice water (0 °C). The final weight-average molecular weights (M_w) of the molded samples were about 25,000 and 13,000 g/mol, respectively. The decrease in the molecular weight was due to the process of hydrolysis in the atmosphere instead of thermal decomposition. The molded samples were thought to be 'amorphous', having no detectable crystallinity (by X-ray and DSC). We came to this conclusion after the following examinations, Geil et al. reported the presence of ordered domains with size of 75–100 Å in ice-quenched PET [3,4]. We found that the peak position of nematic structure in cold drawn PET was different from that of isotropic PET in WAXD image. In addition, we did not observe any SAXS pattern corresponding to a structure of 75–100 Å considering the nematic phase should have a higher density than the isotropic amorphous phase. Thus, we believe that the amount of nematic structure, if any, was quite small in our samples and the initial structure was almost amorphous.

2.3. Experimental procedures

During simultaneous deformation and X-ray measurements, the sample was mounted carefully in an environmental chamber of the Instron instrument, which was heated by hot air. The dumbbell-shaped sample was kept in the chamber for 3 min after being heated to the desirable temperature (90 °C) before engaging tensile deformation. The deformation process was continued until the sample broke. The load–strain curve was recorded simultaneously during the collection of WAXD signals. A separate sample of the same molecular weight was also studied in the chamber at 90 °C without deformation for 40 min to make sure that the sample did not thermally crystallize during the period of the deformation study. A time-averaged WAXD image was collected from the undeformed sample, which was used as a reference for the amorphous phase. No crystallization was observed in either sample of different molecular weight after the thermal annealing without deformation.

2.4. WAXD data analysis

A one-dimensional (1D) peak-fitting program (Grams software by Galactic Industries Corporation) was used to deconvolute the crystalline and amorphous peaks from the linear intensity profiles (Fig. 2) extracted from the 2D WAXD patterns in Fig. 1. Each peak was fitted by a mixed form of Gaussian and Lorentzian functions, having the following formula:

$$f_{MIX} = (1 - M)f_G(x) + Mf_L(x) \quad (1)$$

where $f_G(x) = H \exp\{-[((x - x_0)/w)^2 (4\ln 2)]\}$ (Gaussian), $f_L(x) = H/4[((x - x_0)/w)^2 + 1]$ (Lorentzian), x_0 = peak position, H = peak height, W = full width at half height, and M = mixture (% Lorentzian).

The position, half-width and integrated area of the fitted crystalline peak were used to determine the *d*-spacing, crystal size and fraction of crystalline phase. The azimuthal profiles at two chosen diffraction angles (to be discussed later) were used to estimate the Hermans' orientation function. The procedures for these analyses can be briefly described as follows. During deformation, the sample was semi-crystalline and partially oriented, which was assumed to contain three distinct phases: (1) oriented crystalline, (2) oriented mesomorphic, and (3) un-oriented amorphous phases. The mass fractions of the three phases were estimated from two linear intensity profiles, taken along the equatorial and meridional directions from the 2D WAXD pattern, respectively. The amount of the oriented crystalline phase was assumed to be proportional to the total area of the deconvoluted (100), (010) and (−110) peaks from the linear equatorial profile, whereas, the amount of the un-oriented amorphous phase was assumed to be proportional to the area of the linear meridional profile. (If a crystal diffraction peak was detected in the meridional scan, as the (−103) reflection at high strains, its contribution was excluded. Similarly, contributions from the off equatorial peaks were also eliminated in the analysis.) The subtraction of the crystalline and amorphous fractions from the total area in the equatorial profile was proportional to the amount of the mesophase. The mass fraction of the individual phase was taken as the ratio of the area for each phase to the total area of the equatorial profile [18,19]. The effect of the orientation of mesophase and crystalline phase were totally ignored. As a result, these fractions should be overestimated (results in Fig. 3(b)).

Crystalline dimensions normal to the (100), (010), (−103) reflection planes were estimated using the Scherrer equation [20].

$$D_{hkl} = K\lambda/(\beta_{1/2} \cos\theta) \quad (2)$$

In Eq. (2), D_{hkl} represents the apparent lateral crystallite size of the hkl reflection plane, $\beta_{1/2}$ is the full width at the half height of the diffraction peak hkl in radians, the shape factor K is set at 0.9 for polymer systems, λ is the X-ray wavelength, and θ is half of the diffraction angle. We recognize that there is the possibility of lattice distortion, which would broaden the line width, leading to the underestimation of the crystal size. However, this possibility could not be verified in this work due to the lack of suitable higher order reflections for evaluation. According to Salem [8], the contribution of the lattice distortion is likely to be small. Strictly

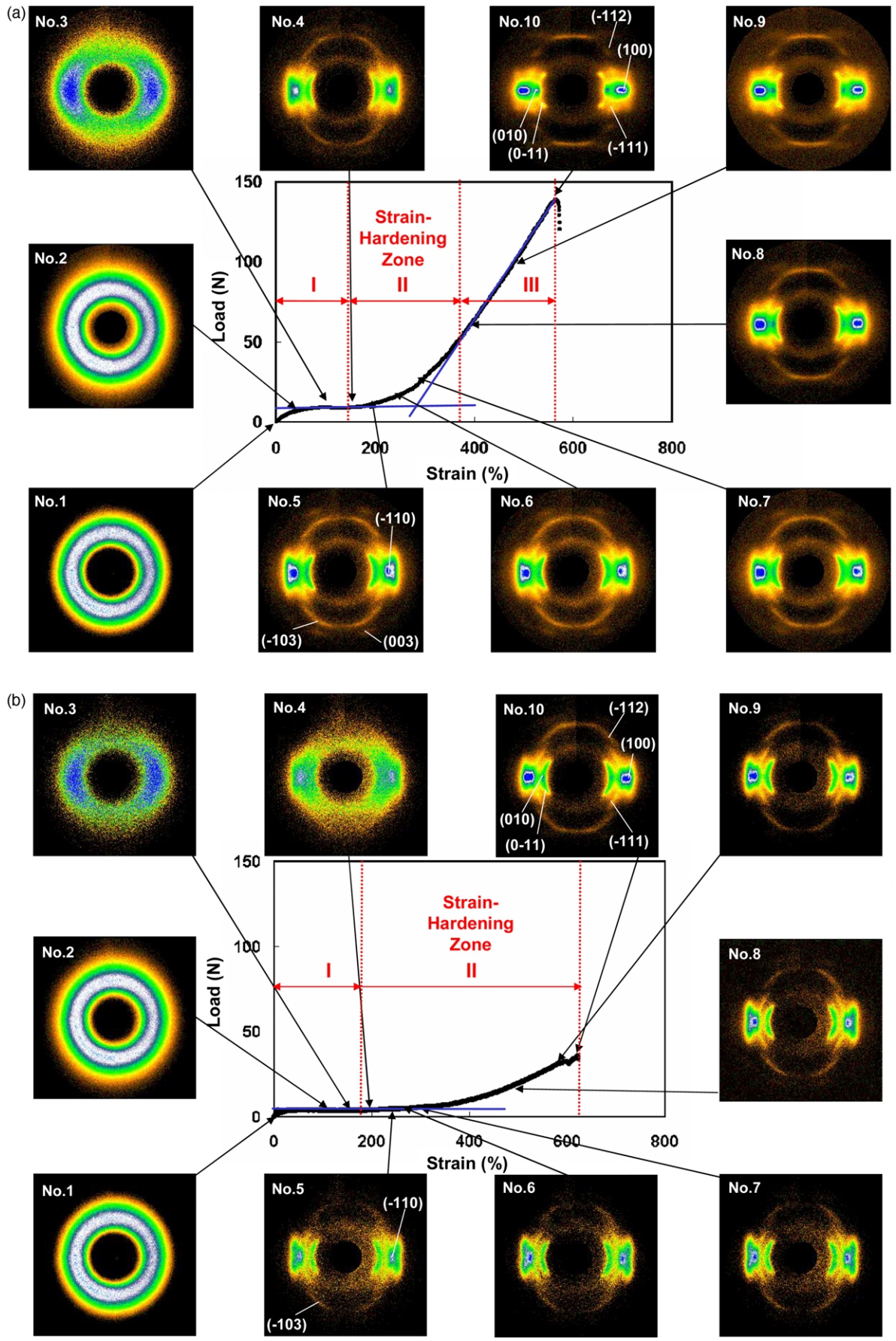

Fig. 1. Load–strain relationship and selected WAXD patterns collected during stretching of (a) higher molecular weight PET and (b) lower molecular weight PET. Each image was taken at the average strain indicated by the arrows. Images No. 1 and 2 in both Fig. 1(a) and (b) are original WAXD patterns without corrections, while the remaining WAXD images are corrected images after the subtraction of the isotropic amorphous phase.

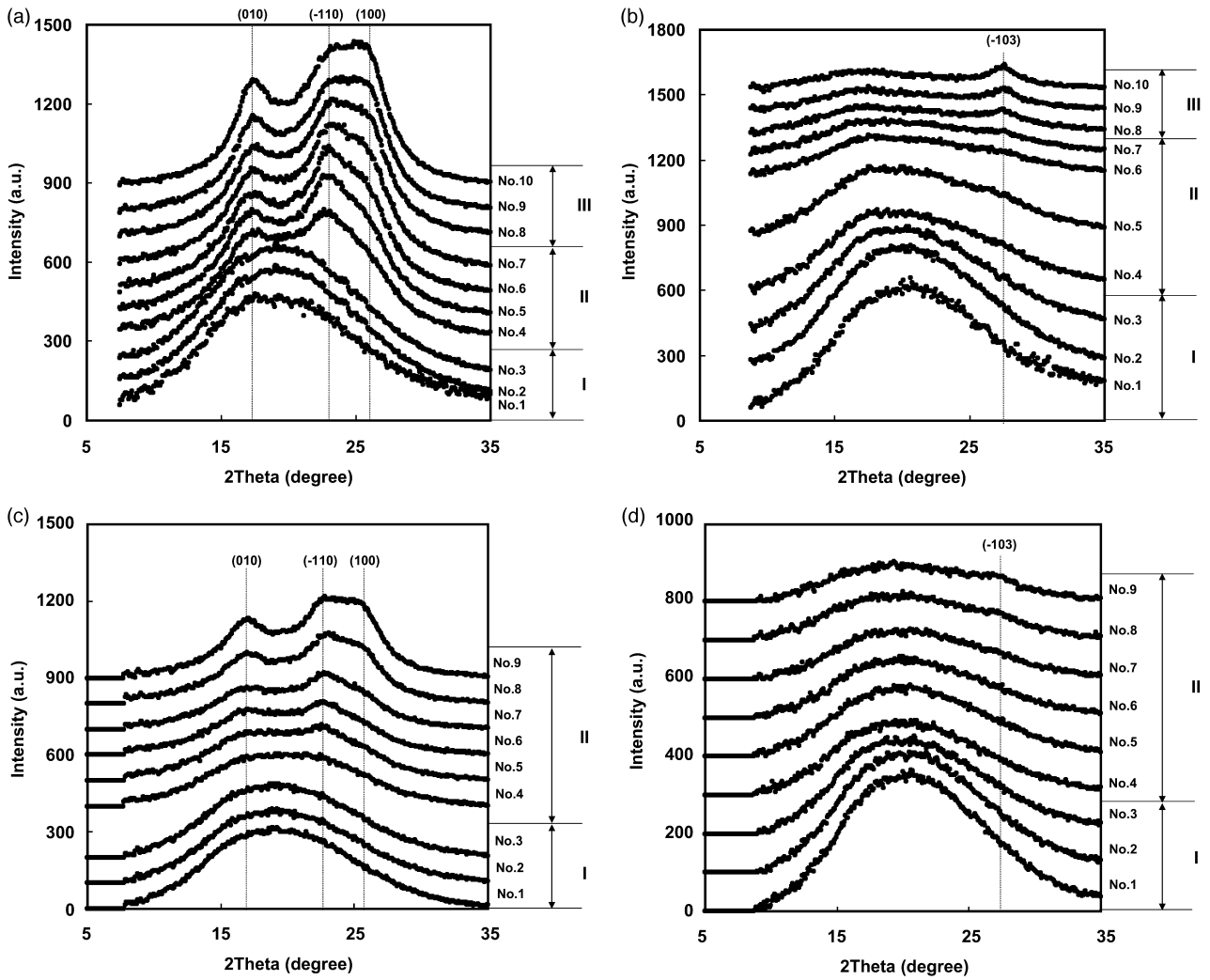

Fig. 2. (a) Equatorial and (b) meridional linear intensity profiles extracted from the 2D WAXD patterns of high molecular weight sample A. (c) Equatorial and (d) meridional linear intensity profiles extracted from the 2D WAXD patterns of low molecular weight sample B.

speaking, the analysis by the use of inverse integral peak widths should be recommended to determine the crystalline size. In view of the fact that the Scherrer equation is a widely adopted method to estimate the crystalline size, we have also used this method to estimate the trend of the crystal size change instead of determining the real value.

The average crystal orientation and its distribution were calculated from the azimuthal scans $I(\phi)$ of two principle equatorial peaks (100) and (010) [20], where ϕ represented the azimuthal angle (note that we defined the position $\phi = 0$ to be the meridional direction instead of the equatorial direction). Because PET has a triclinic crystalline unit cell with the 100 and 010 planes tilted against the molecular axis, these peaks can split into two along the azimuthal direction near the equator. Each (100) and (010) reflection was assumed to contain a doublet near the equator at intermediate strains (e.g. at strains less than 400% in the sample A and less than 500% in the sample B), and was analyzed using the mixed function described in Eq. (1). At higher strains (i.e. $>400\%$ in sample A and $>500\%$ in sample B), as the Grams program could no longer deconvolute the measured peak, the analysis was carried out by assuming that only one diffraction peak was present on the equator. The crystal orientation was determined by the Hermans' orientation function (f_{Hermans})

$$f = \frac{3\langle\cos^2\phi\rangle - 1}{2} \tag{3}$$

where $\langle\cos^2\phi\rangle$ was defined as

$$\langle\cos^2\phi\rangle = \frac{\int_0^{\pi/2} I(\phi)\cos^2\phi\sin\phi\,\mathrm{d}\phi}{\int_0^{\pi/2} I(\phi)\sin\phi\,\mathrm{d}\phi} \tag{4}$$

The above analysis requires the specimen to possess a cylindrical symmetry, which may not be the case for the film

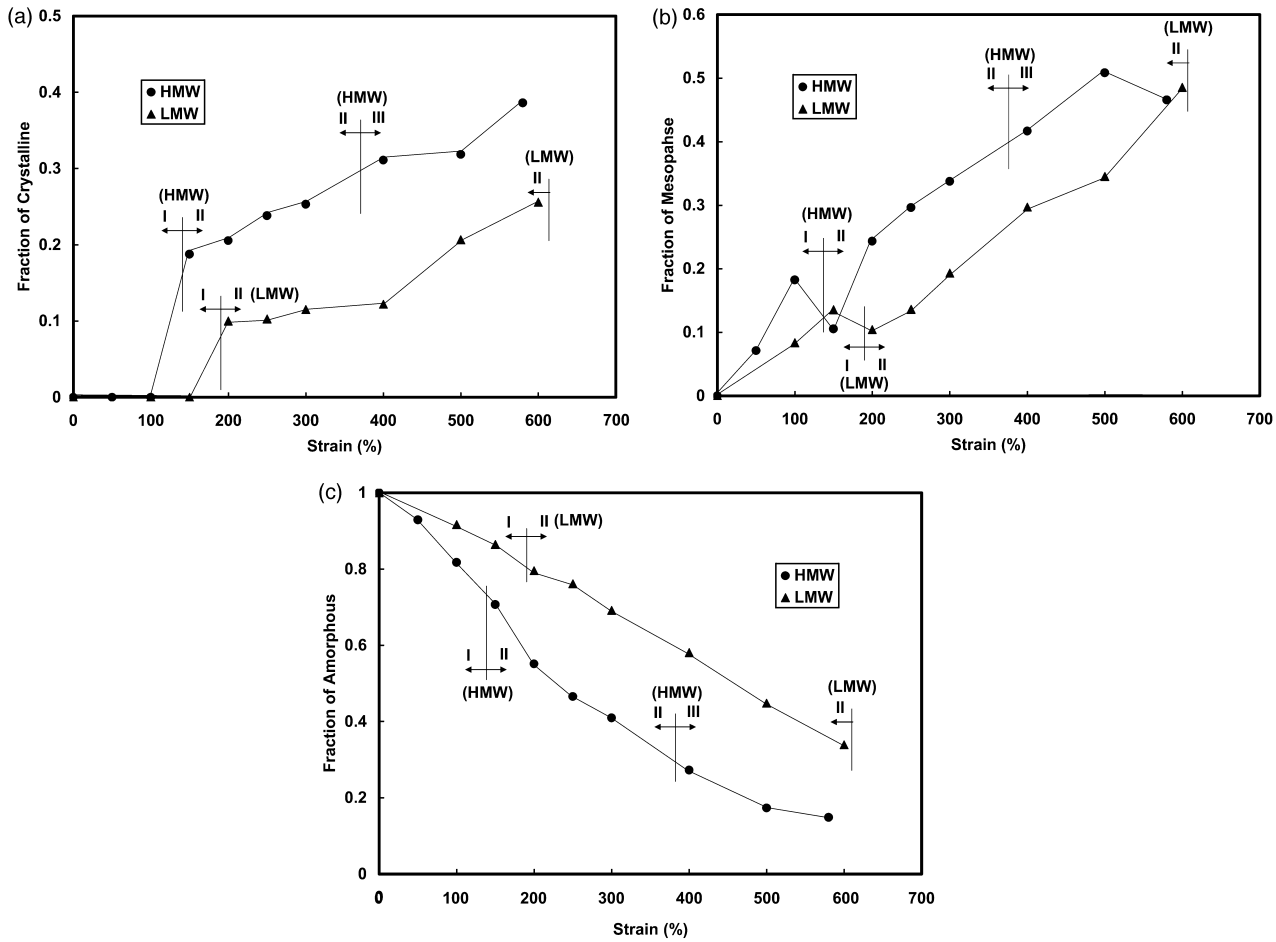

Fig. 3. Mass fractions extracted from the two linear intensity profiles of high molecular weight sample A and low molecular weight sample B: (a) oriented crystalline phase, (b) oriented mesophase and (c) unoriented amorphous phase.

geometry encountered in this study. It is well known that in typical crystalline PET film, the (100) reflection has a tendency to align its normal parallel to the film surface. [21,22] To address this concern, we have taken 2D WAXD patterns along the face-on as well as the edge-on directions from both deformed samples. Our results indicated that the WAXD patterns along these two directions were similar and both deformed samples could be assumed to have a cylindrical symmetry. Perhaps, this is because the initial samples were amorphous instead of semi-crystalline. No orientation factor was determined from the (−103) diffraction peak near the meridian.

We also performed the Fraser correction to convert the flat-plate WAXD image into the data in undistorted reciprocal space [23]. The procedure allowed us to follow the changes of the unit cell parameters during deformation. This is because the meridional scans of the uncorrected 2D patterns are not true meridional scans but curved profiles in the reciprocal space. The exact positions of the peaks, especially for those near the meridian, were determined after the Fraser correction. We have recently demonstrated this procedure in the PET deformation study below T_g [16].

3. Results and discussion

From our earlier deformation study of the amorphous PET film below T_g [16] and the current cursory evaluation of the WAXD images through both face-on and edge-on directions, we concluded that the structure developed from the deformed amorphous sample in this study exhibited a rough cylindrical symmetry (this would not be correct if the starting film was semi-crystalline). This assumption significantly simplified our data analysis schemes. The resulting structural information, although semi-quantitative, turned out to be quite useful for the understanding of the mechanism for structural development during deformation of PET above T_g.

The load–strain curves and selected WAXD patterns (through the face-on direction) taken during uniaxial deformation of the two PET samples are shown in Fig. 1 (A for the higher molecular weight sample and B for the lower molecular weight sample). Images No. 1 and No. 2 in both Fig. 1(a) and (b) are original WAXD patterns without correction, while the remaining WAXD images are corrected images after the subtraction of the isotropic amorphous phase. The two load–strain curves were

obtained under the same experimental conditions. Overall, both curves exhibited a similar trend of increase, except for the exact values of strain hardening and of strain at break. The corresponding WAXD patterns for each sample under the same experimental conditions were somewhat different, indicating that the structural development during deformation is molecular weight dependent. This will be discussed in more detail later. We note that the high intensity of the synchrotron X-rays made it possible to collect the WAXD patterns during stretching in real time without holding. As the acquisition time for the X-ray detection was 20 s per image, each WAXD pattern represented an average structure occurring during deformation in a 6.7% strain span. In Fig. 1, the arrow indicated the average strain value, where each WAXD image was taken. It was seen that only the initial WAXD image was isotropic, the rest of the WAXD images taken from the deformed sample were anisotropic with orientation increased with strains.

In a recent communication [24], we proposed that the structural development during uniaxial deformation can be divided into three zones: I—the region before strain-hardening, II—the strain-hardening region, and III—the region after strain-hardening. Each zone contains distinct features in the structural development. This three-zone argument resembles the three-staged classification proposed by Gorlier et al. [9] using the step-quenching technique. However, the mechanism of structural formation in each 'zone' is quite different from that in each 'stage' (we note that the use of 'zone' versus 'stage' is only semantic, which is intended to indicate the different mechanism from the different study). Thus, the extraction of the detailed molecular information in each zone during uniaxial deformation is the primary theme of this paper.

In the conventional view, the determination of the strain-hardening point on the load–strain curve can be made by the interception of two extrapolated lines: one fitting the load–strain curve in the low strain region (not including the initial load increase at strain less than 50%), and the other one fitting the load–strain curve in the high strain region (see Fig. 1(a)). The cross-point of the two lines marks the initiation of the strain-hardening process. The corresponding mechanical property is often divided into two parts for discussion, before and after the strain-hardening point. However, this approach is not consistent with the evolution of microstructure observed by in situ WAXD results in Fig. 1. For one, there was no abrupt phase transition at the strain-hardening point (the crystallization occurred much earlier than the strain-hardening point). A more proper way to correlate the structure and the strain-hardening behavior is by using the definition of a strain-hardening zone, which starts from the first deviation point of the fitted line in the low strain region and ends with the none deviation point of the fitted line in the high strain region (see Fig. 1(a)). In the following sections, we will carefully describe the microstructures formed in each zone. These microstructures include the fractions of crystalline, mesophase and isotropic amorphous phases, crystalline size, *d*-spacing of the crystalline lamellar structure, average crystalline tilt angle and so forth. In addition, we will compare the difference between the systems of high molecular weight (HMW) and low molecular weight (LMW) PET samples.

3.1. Zone I—mesophase development before strain-hardening

In Zone I (strain less than 140%), three WAXD images (Nos. 1–3 in Fig. 1(a)) were collected in the sample A (the HMW sample). The No. 1 WAXD pattern was taken before the deformation process, which showed only an amorphous ring confirming that the initial structure in the quenched PET sample was amorphous without preferred orientation. Upon deformation, a small increase in load was seen. This load remained at a constant level (8 N) in the remainder of Zone I until the onset of the strain-hardening Zone II (ca. 140% strain) was reached. The region of the constant load is often referred to as the 'plastic deformation' region. Two more WAXD images were taken (Nos. 2 and 3) in this region. The No. 2 WAXD image showed a very weak trace of anisotropy near the equator. In contrast, the No. 3 image showed a distinct pattern of the oriented mesophase in PET, i.e. the scattered intensity was seen to converge into a pair of broad and intense arcs on the equator. The mesophase structure has a degree of packing order that is between the crystalline phase and the amorphous phase. Although we cannot determine the exact type of mesophase in the deformed sample, we speculate that the strain-induced mesophase may be nematic or smectic C as recently identified in our study of the amorphous PET deformed below T_g [16].

The load–strain relationship and the corresponding structural changes in Zone I can be explained by the following argument. The increase in the initial load represents the force needed to overcome the activation energy for polymer flow at the experimental temperature (90 °C) [25]. In this zone, even if some polymer chains are stretched, the fraction of oriented chain segments is low and the degree of molecular orientation is also low, resulting in the weak appearance of anisotropy in the WAXD pattern. In the plastic deformation region, as the activation energy for continuation of orienting the chain segments remains about constant, the applied load also stays constant. However, as strain increases both the fraction of oriented chain segments and the degree of molecular orientation increase, the deformation process eventually produces a distinct anisotropic WAXD pattern indicating a mesomorphic structure. In other words, in the plastic deformation zone, the concentration of the oriented mesophase increases continuously with strain, in spite of the constant load. It is known that the average orientation is proportional to stress (load divided by the cross section area of the sample). If we assume the density of the sample is constant in Zone I, the cross section area then decreases inversely, proportional to strain. As a

result, stress increases proportional to strain under the constant load. This suggests that the fraction of the oriented mesophase increases linearly with strain in accord with the stress-optical law. The result shown in Fig. 3(b) fully supports this argument.

A similar behavior was also observed in the LMW sample B (Fig. 1(b)). Comparisons of the load–strain relationships and the structural developments between the high and low molecular weight samples (Fig. 1(a) and (b)) yielded several interesting findings. First, the plateau load value in the plastic deformation zone for the LMW sample was lower than that for the HMW sample (5 N versus 8 N). Second, the final strain value of Zone I for the LMW sample was higher than that for the HMW sample (180% versus 140%). Third, at the same strain level, the observed oriented mesophase pattern was weaker in the LMW sample, indicating that a lower concentration of the mesophase was obtained. These findings can be explained by the following argument. In this study, the initial PET sample was an amorphous glass without crystallinity. Above T_g, the PET glass became PET melt where the 'flow draw' phenomenon was seen. This behavior has been reported before [26–27]. The plastic deformation of PET above its T_g could be treated as the flow of a viscoelastic polymer melt. In the LMW sample, the corresponding activation energy for elongational viscosity is lower than that of the HMW sample. (The relationship between the viscosity and the molecular weight during elongational flow of PET melt has been clearly described by George using the constitutional equation [28]). As a result, the plateau load value in the plastic deformation zone is lower in the LMW sample. Since the melt viscosity is also proportional to the relaxation time spectra of the chains, the LMW sample (with lower viscosity) has a larger population of chains with shorter relaxation times [29]. This will result in the generation of a lower fraction of the mesophase for the LMW sample under the same straining conditions during plastic deformation than that for the HMW sample, which was clearly detected by WAXD. It is well known that the chains of short relaxation times cannot remain in the oriented (or stretched) state under deformation [30,31]. Consequently, the amount of mesophase and the corresponding load are lower in the LMW PET sample.

The WAXD images, No. 3 in Fig. 1(a) and No. 3 in Fig. 1(b), indicate that only a small fraction of the oriented mesophase is produced in Zone I. This can be explained that only the chains with relaxation times longer than a critical value can remain oriented after stretching; while the rest of the chains are relaxed and return to the isotropic state. Recently, we reported that this critical value of relaxation time is probably inversely proportional to the deformation rate [30] and should be a strong function of temperature and strain. The precise relationship between the critical relaxation time, above which the chains can retain orientation after deformation, as a function of strain, strain rate and temperature, will be a subject for our future study.

Gorlier et al. [9] have correlated the plastic deformation zone to the chain orientation process. We generally agree with their viewpoint. However, we want to point out that the chain orientation process induces the formation of mesophase, which is a first-order phase transition. Even though the fraction of the mesophase produced in this zone can be low (thus not easily detectable by WAXD), the role of the mesophase is critical for the initiation of nuclei. Once the nuclei are formed, the crystal growth process will also be facilitated by the orientation of the chains in the mesophase region. The processes of nucleation and growth take place in the early stages of Zone II.

3.2. Zone II—structural development during development of strain-hardening zone

In the HMW sample, the strain-hardening zone began at 140% strain and ended at about 380% strain (the corresponding WAXD images collected during this zone range from Nos. 4 to 7 in Fig. 1(a)). In the No. 4 image, a clear indication of crystallization in the WAXD pattern is seen, which coincides with the initiation of strain hardening. This should not be a surprise, as in our early deformation study of amorphous PET below T_g [16] and the studies by Gorlier et al. [9] and Chaari et al. above T_g, [15] we noted that the mesophase behaved as a precursor for strain-induced crystallization, i.e. the strain-induced crystallization occurred mainly in the mesophase region. We believe that the similar behavior also took place here during deformation above T_g. The incremental structural changes from Nos. 4 to 7 offered us a unique opportunity to examine the mechanism of crystallization from the oriented mesophase.

Both equatorial and meridional intensity profiles extracted from the flat-plate 2D WAXD pattern of the HMW PET sample are illustrated in Fig. 2(a) and (b), respectively. In Fig. 2(a), two distinct equatorial reflection peaks and a weak higher angle shoulder were identified in the No. 4 profile. These peaks could be indexed as the (010), (−110), and (100) reflections, respectively, based on the triclinic unit cell structure in PET [32]. From the meridional profile (Fig. 2(b)), no diffraction peak could be identified until the end of Zone II (profile No. 7), where the (−103) peak (d-spacing = 2.96 Å) was seen. We noticed that the (−103) peak was in fact visible in all 2D WAXD images in this zone (e.g. No. 4 in Fig. 1(a)). The missing (−103) peak in the meridional scans was because this peak was not located on the meridian until the end of Zone II. Thus, the extracted meridional profiles (in Fig. 2(b)) in the early stages of Zone II represented the contributions of the unoriented amorphous phase at different strains. The appearance of the (−103) peak in the No. 7 profile (in Fig. 2(b)) was due to the increase in crystal perfection and orientation at a higher strain. In the No. 4 WAXD image of Fig. 1(a), four (003) peaks at a higher angle (d-spacing 3.10 Å) near the meridian were also seen. As they were also located at some off axis angles with respect to the meridian, they could not be viewed from the linear meridional scan.

The general features of the WAXD patterns in Fig. 1 have also been observed before in several step-quenching deformation studies, as carried out by Schultz et al. [33], Salem [8], and Gorlier et al. [9].

Extracted equatorial and meridional intensity profiles from the 2D WAXD pattern of the LMW PET sample are illustrated in Fig. 2(c) and (d), respectively. Overall, the diffraction features observed in the LMW sample were similar to those in the HMW sample. Three equatorial peaks, which could be indexed as (100), (010) and (−110), were seen to increase in Zone II, where the (−103) peak on the meridian was also identified only at the end of Zone II (profile No. 9). Unfortunately, no Zone III was seen in the LMW sample. In other words, the LMW sample broke (strain ≈620%) before the occurrence of Zone III. This is not surprising as the sample breakage during tensile deformation is usually related to the chain pull-out from the craze surface. As the molecular weight of the sample is decreased, the entanglement between the chains becomes less and the pull-out breakage becomes easier. As a result, the stable crystallization growth in Zone III (to be described later) is not achievable by the uniaxial deformation of LMW sample.

The No. 4 WAXD pattern of the HMW sample (Fig. 1(a)), representing the initial crystalline structure, exhibited several distinct diffraction peaks around both equator and meridian axes. This pattern was generally consistent with the triclinic crystal structure of PET, although the corresponding unit cell dimensions were quite different than the typical values [32,34]. In the No. 4 pattern, the strongest two peaks were (010) and (−110) reflections near the equator, which indicated that the initial crystalline structure was dominated by the formation of an inter-chain benzene sheet structure (which would result in a strong 010 peak) instead of a benzene stacking structure. Here the benzene sheet structure indicates that the planes of benzene rings are on the same plane, whereas, the benzene stacking structure indicates that the planes of benzene rings pile up as layers. The preferential growth of the 010 reflection in PET during stretching was reported earlier by Salem [8] and Huisman [35] and our results agreed well with their findings. However, our results did not support the argument by Gorlier et al. [9], who stated that the initial crystalline structure induced by tensile deformation had only two-dimensional (2D) ordering. This is because they did not observe the presence of the (−103) peak in their study. We believe that their observation was probably due to the use of the lower molecular weight sample (M_w = 19,000 g/mol). In the study of sample B (M_w = 20,000 g/mol), we also could not identify the (−103) peak in the uncorrected (as-measured) No. 4 image in Fig. 1(b). However, after the subtraction of the amorphous background, the No. 4 image in Fig. 1(b) exhibited a weak but clear presence of the (−103) peak. This indicated that the initially formed crystalline structure induced by stretching had distinct three-dimensional ordering, although the ordering along some axes was relatively poor.

Using the method described earlier, the fractions of the oriented crystalline, oriented mesomorphic and random amorphous phases were estimated, and the results are shown in Fig. 3(a)–(c), respectively. The levels of the mesophase and crystalline fractions in the HMW sample were consistently higher than those in the LMW sample (the amorphous fraction thus was lower). However, these three figures revealed several new but consistent features for both HMW and LMW samples. (1) The amorphous fraction decreased continuously in the entire process of deformation. (2) In Zone I, only the oriented mesophase was developed, which increased with strain. (3) In Zone II, the crystalline phase appeared but the corresponding mesophase fraction decreased upon the initiation of crystallization. This observation, seen in both HMW and LMW samples, suggested that the fraction of the mesophase was consumed by the formation of the crystalline phase, which supported the argument that the mesophase acts as a precursor for crystallization and crystallization occurs mainly in the mesophase region. In addition, the development of the crystalline phase coincided with the increase of the load, which marked the beginning of the strain-hardening zone. The similar behavior was also reported in the study of high speed spinning for PET [18,19]. (4) Upon further deformation, both fractions of the mesophase and the crystalline phase increased continuously with strain (in Zones II and III). The amount of the mesophase was consistently higher than that of the crystalline phase in the deformed samples (see Fig. 3(a) and (b)).

The apparent crystal sizes normal to the three crystal reflections: (100), (010) and (−103), were estimated by the analysis of the linear intensity profiles taken across the reflection peaks using the Scherrer equation (Eq. (2)). These results are shown in Fig. 4(a) and (b) for HMW and LMW samples, respectively. The estimated sizes were probably underestimated because there were several factors such as instrumentation broadening and thermal fluctuations that could broaden the diffraction peak. The effect of thermal fluctuations might be particularly significant since the measurement was carried out at 90 °C. The three chosen reflections ((100), (010) and (−103)) are almost orthogonal to each other, thus marking the average lateral sizes of the crystals induced by deformation. In both Fig. 4(a) and (b), the size normal to the 010 plane was the largest, which represented the dimension related to the benzene sheet formation. The size normal to the −103 planes was the smallest at the beginning of Zone II, which indicated the dimension (or the coherent length) developed along the chain-axis (the *c*-axis) was relatively small. However, this size increased more rapidly in the latter part of Zone II than those of the 100 and 010 planes. This suggests that the lateral interactions between the 010 and 100 planes probably formed first, which initiated the crystallization and allowed the growth of the −103 plane (or longitudinal ordering)

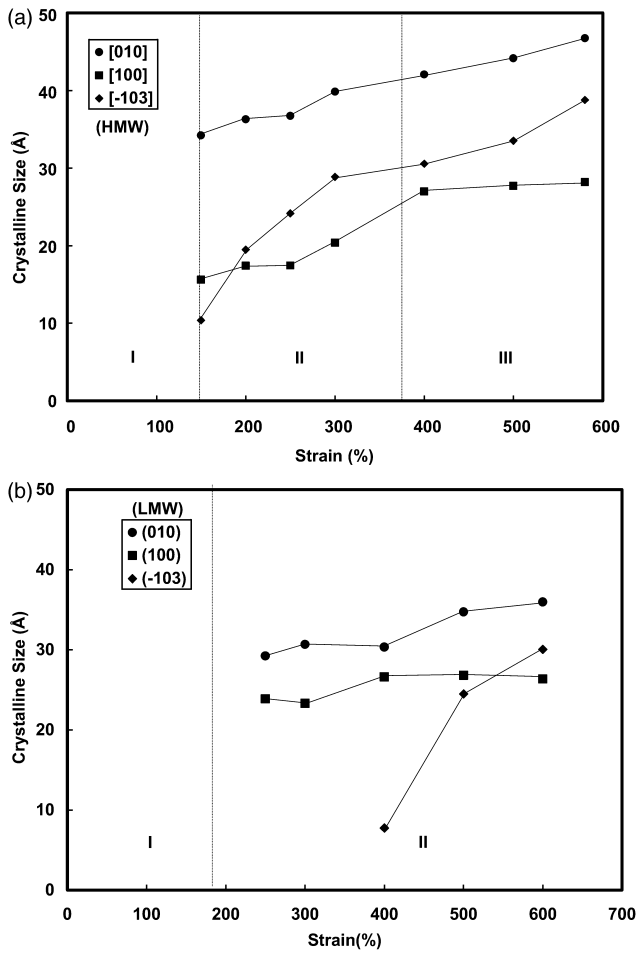

Fig. 4. Estimated crystal sizes from three nearly orthogonal reflection planes: (a) (010), (100) and (−103) of high molecular weight sample A during deformation: (b) (010), (100) and (−103) of low molecular weight sample B during deformation.

along the chain axis. This behavior was seen in both HMW and LMW samples (Fig. 4(a) and (b)). The estimated sizes for the HMW sample are higher than those for the LMW sample, which are consistent with the crystal fraction results in Fig. 3. The size of the initial crystalline structure was quite small. For example, the crystalline size at the beginning of Zone II in HMW was 33 Å for the (010) reflection and 14 Å for the (100) reflection. The number of repeating unit corresponding to the crystalline size was calculated to be 6.3 for (010) and 3.8 for (100). This indicates that the initial crystalline structure is consisted of only a few interacting chains.

The *d*-spacings for the three principal (100), (010) and (003) reflections were calculated using Bragg's law, and the results are shown in Fig. 5(a)–(c), respectively. In the HMW sample, it was seen that the *d*-spacings of both (100) and (010) reflections decreased with strain with the largest reduction taking place in the later part of Zone II. In contrast, the *d*-spacing of the (003) reflection increased with strain. In the LMW sample, the *d*-spacing of the (010) reflection also decreased sharply with strain in Zone II, but the *d*-spacing of the (100) reflection remained about constant. The (003) peak was not clearly seen in the LMW sample. The large reduction of the (010) *d*-spacing suggests that the interactions between the benzene ring stacking were quite poor in the initial stage of crystallization in Zone II, which was seen in both samples. In Fig. 5, the comparison also shows that the crystallization took place at higher strains and lower stress levels for the LMW sample than those for the HMW sample. It is interesting to note that no significant *d*-spacing decrease of the (100) peak in the LMW sample was seen. This indicates that the crystal perfection process during deformation becomes unfavorable with the decrease in the molecular weight. The decreases in two lateral *d*-spacings of (100) and (010) and the increase in the *d*-spacing of (003) could be attributed to the changes mainly in two unit cell parameters (α and β angles, both are related to the chain axis alignment). The parameters of a, b, c and γ were found to remain constant during deformation. This behavior has been described by us elsewhere [24].

The deformation process also affected the average orientation and the orientation distribution of the crystallites, as indicated by the narrowing of the azimuthal spread with strain. The azimuthal peaks were analyzed by the peak fitting method. The average orientation was determined by the position of the azimuth peak and the orientation distribution was estimated by the full-width at the half height (FWHH) of the peak. The peak displacements or FWHH of equatorial (100) and (010) peaks for the HMW and LMW samples are shown in Fig. 6. Both samples exhibited noticeable decreases in the peak displacement with strain, indicating the increase of crystal orientation in Zone-II. However, the decrease of the displacement in the HMW sample was found to be significantly larger than that in the LMW samples. This indicated that the crystal orientation induced by drawing in the LMW sample was significantly lower than that in the HMW sample.

The Hermans' orientation functions (f) calculated from the deconvoluted azimuthal peaks of the two principal diffraction peaks (010) and (100) are shown in Fig. 7(a) and (b), respectively. It was seen that the f value associated with the (010) peak increased with strain, but that associated with the (100) peak remained about constant ($f = 1$ represents the perfect orientation) in the HMW sample. The orientation function of the (100) peak was higher than that of the (010) peak. This result indicates that there were more long-range interactions within the polymer chains in the 010 plane than with those in the 100 plane. This conclusion is also consistent with the observation of the higher crystal thickness value with respect to the 010 plane (Fig. 4). A similar behavior was seen for the LMW sample. The orientation function of the (100) peak was higher than that of the (010) peak. The *f*-value associated with the (010) peak also increased with strain in the LMW sample, but its starting value was higher than that in the HMW sample.

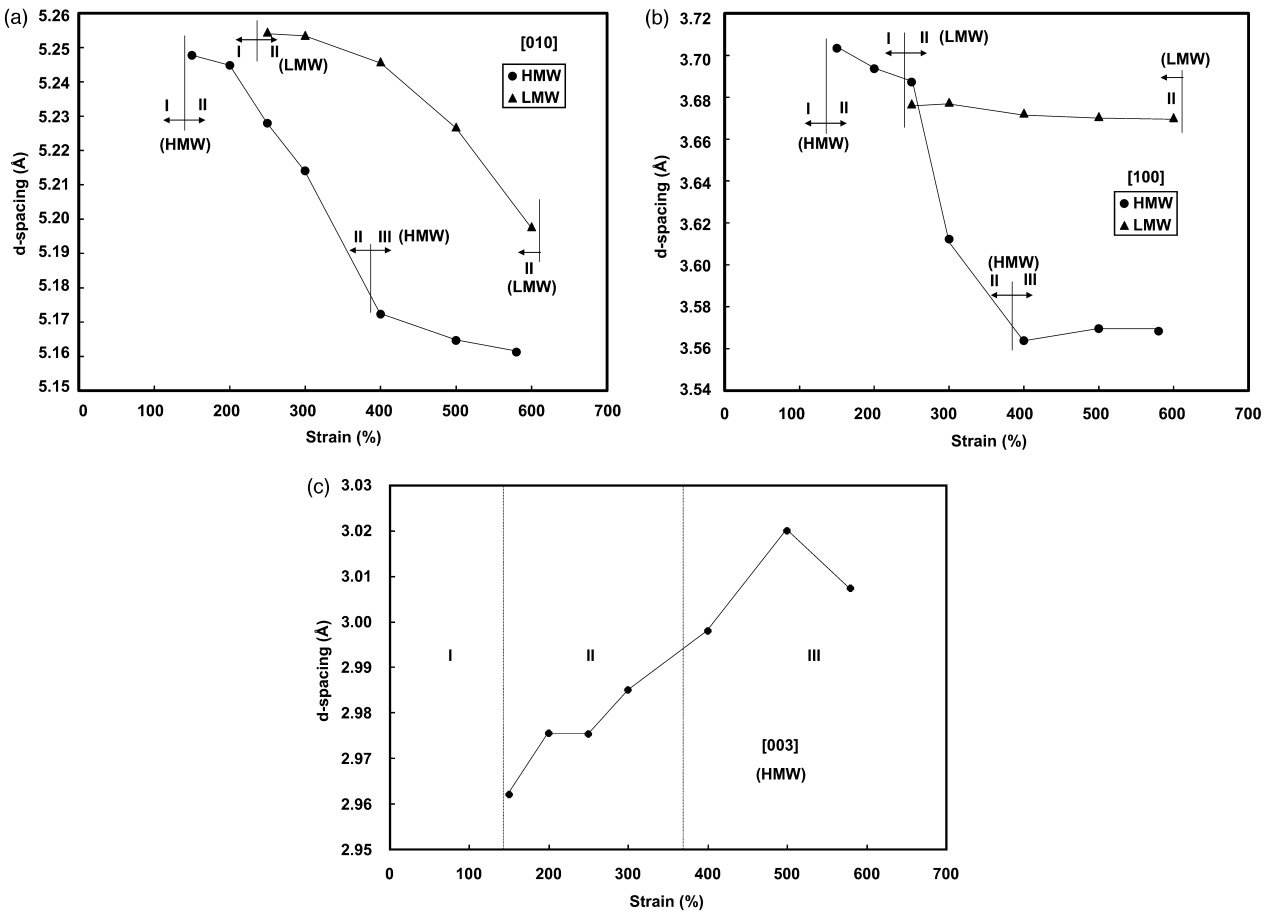

Fig. 5. Changes of *d*-spacing during deformation above T_g for (a) (010), (b) (100) and (c) (003) diffraction peaks.

3.3. Zone III—structural development after strain-hardening zone

In the HMW sample of Fig. 1(a), the region of strain hardening (Zone II) ended at a strain of 380%. A constant load–strain ratio was observed afterward, marking the unique feature of Zone III. Zone III began at the 380% strain and ended at the break point for the HMW sample (the maximum strain was about 580% and the maximum load was about 135 N). In contrast, for the LMW sample (Fig. 1(b)), Zone III was not observed (the break point at the maximum strain of 620% and the maximum load of 37 N was still in Zone II). The maximum load of the LMW sample (37 N) was substantially lower than that of the HMW sample (135 N). This is consistent with the argument that the strength of the sample is inversely proportional to the number of chain ends. In other words, as the molecular weight decreases, the number of chain ends increases, reducing the concentration of tie chains between the adjacent crystallites and thus the final tensile property [36,37]. It is logical to assume that the mechanism responsible for the sample breakage is mainly due to the pull-outs of the chains, as the typical maximum strength of a polymer is substantially lower than the theoretical value of the broken chains. The higher the tie-chain concentration present between adjacent crystallites; the higher the load required to break the sample. Although the WAXD data cannot be used to detect the tie chains between the crystallites, it can be used to reveal the crystal structural

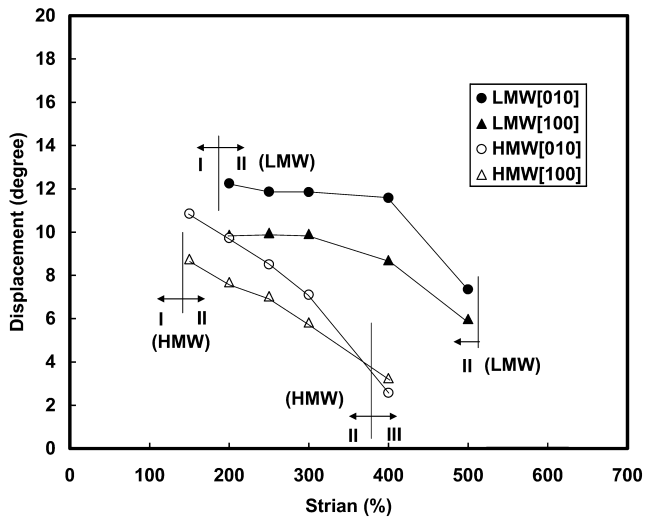

Fig. 6. Displacement angles of three selection diffraction peaks ((100) and (010)) during deformation.

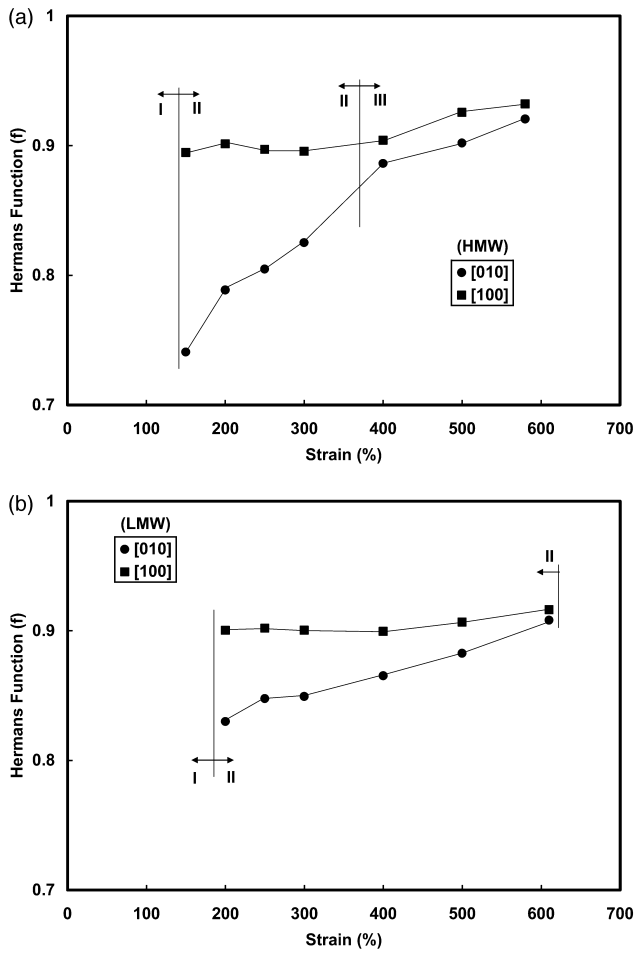

Fig. 7. Changes of Hermans' orientation function during deformation of PET above T_g: (a) high molecular weight sample A (b) low molecular weight sample B.

development and its relationship with the mechanical property during deformation in Zone III, as depicted below for the HMW sample.

In Fig. 3, the mass fraction of the amorphous phase was seen to decrease continuously, while the fractions of both crystalline phase and mesophase all increased with strain. The amount of the mesophase was consistently larger than that of the crystalline phase. These findings indicated that, in Zone III, the production of the mesophase was proportional to the increase in strain. As crystallization could only be initiated within the mesophase, the resulting crystalline fraction continuously lagged behind the mesophase fraction, even at the break point (strain = 580%). In a previous study [16], we demonstrated that if the elongation was stopped and the temperature was raised under a constant strain, only the mesophase could be converted into the crystalline phase because both isotropic and anisotropic contents remained constant.

In Fig. 4(a), the apparent crystal sizes for the three reflections: (010), (100) and (− 103) all increased with strain in Zone III. The rate of the increase associated with the size of the (− 103) peak was the largest among the three. It is interesting to note that in the sizes associated with the (100) and (− 103) peak, there appeared to be a break point between Zone II and Zone III. The slope of the size increase (by strain) in Zone II was larger than that in Zone III. However, this was not seen in the size of the (010) peak, where the slope was the same for Zone II and Zone III. Such a transition behavior was also observed in the *d*-spacing plots (Fig. 5(a)–(c)). The changes of the *d*-spacings in Zone III were quite small, compared with those in Zone II. This suggests that the process of crystal perfection was largely completed in Zone II, whereby relatively few structural changes occurred in Zone III. Furthermore, the *d*-spacing of the 100 peak remained constant in Zone III, indicating that the projected spacing between the benzene stacks did not change.

In Fig. 6, the average azimuthal peak width displacements for both (010) and (100) peaks reached a low value at the end of Zone II (displacement less than 3°) and they did not change significantly in Zone III. In Fig. 7, the Herman's orientation function of both (010) and (100) peaks increased almost linearly with strain in Zone III, but with a very slow rate. These results indicate that the crystal orientation in Zone III was slightly improved by drawing, but the majority of the orientation was already accomplished by the end of Zone II. A transition point between Zone II and Zone III was seen in Fig. 7. For example, the Herman's orientation function of the (100) peak was about constant ($f = 0.9$) in Zone II, while it increased to 0.93 by the end of Zone III. In contrast, the Herman's orientation function of the (010) peak increased significantly in Zone II, while the rate of the increase was reduced in Zone III.

In Zone III, our results showed several new findings, which disagree with some conclusions reported in the literature. (1) Gorlier et al. reported that the crystalline growth stage started around the onset of the linear stress development, which coincided with the appearance of the (− 103) peak indicating the perfection of the crystalline structure [9]. Our result indicated that although the crystalline structures in Zone III were significantly 'perfected' when compared with the initial defective crystal structure formed at the beginning of Zone II, they changed continuously with strain. In fact, the ongoing perfection process of the crystalline structure persisted until the breakage of the sample. (2) Salem reported that the increase of crystallinity slowed down at the onset of the linear stress development with density measurement [8]. We did not observe this behavior. In Fig. 3(a), the mass fraction of the phase crystalline was found to increase almost linearly with strain in Zone III. Perhaps, the variation was due to their inclusion of the mesophase as part of the crystalline phase.

3.4. Proposed mechanism for structural development during deformation above T_g

Based on the above results, we can propose a possible

mechanism for the structural development during deformation of amorphous PET above its T_g and its correlation with the mechanical properties as follows. A schematic diagram, using the division of three zones for the HMW sample, as illustrated in Fig. 8, is used to facilitate the discussion.

In Fig. 8, Zone I represents the induction period of oriented mesophase without the actual formation of crystals. In the very initial stage, a small load is needed to overcome the activation energy of polymer flow above T_g to initiate the oriented mesophase. However, during the continuing development of oriented mesophase, the required load remains about constant until the formation of crystals. The higher the molecular weight of the sample, the larger the initial load needs to be overcome, and consequently, the greater the concentration of the oriented mesophase that will be produced. It has been proven that the mesophase provides the nucleation sites for crystallization, i.e. the mesophase acts as precursors to crystallization. The event of nucleation cannot be sporadic in the deformed sample; it probably prefers the region of higher molecular orientation.

Upon the initiation of crystallization, the applied load increases soon after. The deviation from the constant load region marks the beginning of Zone II or the strain-hardening zone. The load increase can be attributed to the formation of a three-dimensional (3D) network of small crystallites, which reinforce the continuum matrices containing random amorphous phase and oriented mesophase. The greater the concentration of the crystallites, the larger the load needed to deform the sample. Moreover, in the initial stage of crystallization, the formed crystals (still with a structure of triclinic unit cell as shown by the presence of (-103)) are quite defective and do not possess good orientation. The crystal registration along the benzene sheet, indicated by the (010) peak, appears to form first. The growth along the benzene stacking direction appears to develop later (at a higher strain). In this zone, several processes appear to proceed simultaneously with the increasing strain: crystal growth along all three directions,

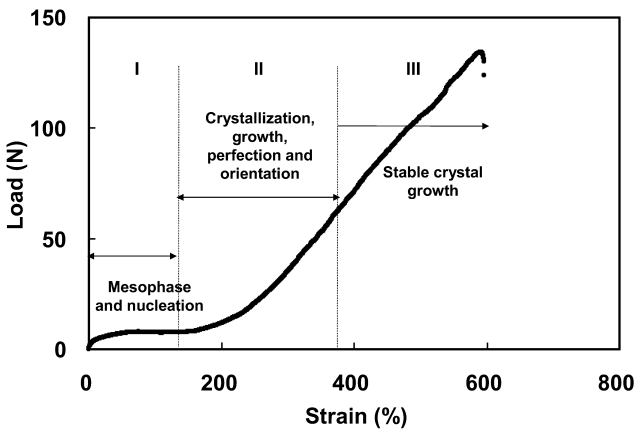

Fig. 8. Proposed mechanism for the structural development and mechanical response during deformation of PET above T_g.

crystal perfection and crystal orientation. The crystal perfection process can be followed by the changes of two unit cell angles (α and β) in the triclinic structure during deformation [24]. We argue that the formation of the crystalline phase mainly occurs in the mesophase, which is consistent with the observation that the mesophase content decreased during the initial development of crystallization. Finally, the end of Zone II can be marked by the stabilization of the crystal structure and concentration, where the load is found to be linearly proportional to strain afterwards.

In Zone III, the ratio between load and strain remains about constant until the break point of the sample is encountered. In this zone, the crystalline structure becomes stable with increasing strain, having good lattice registrations typical of the PET triclinic unit cell reported in the literature. The increase in the load reflects that the crystalline fraction is increased, suggesting the continuation of the growth process. The overall crystal orientation is also found to increase with strain. The molecular weight of the sample appears to have very little effect on the formation of the crystal structure, but it greatly impacts the final strength (maximum load), the fractions of the crystalline phase and mesophase and the initial point of Zone II. The higher performance of the higher molecular weight sample can be attributed to the lower concentration of chain ends and the high concentration of the crystalline phase and mesophase. This is consistent with the conventional notion that the sample breakage under uniaxial deformation is mainly due to the pull-out of the chains.

4. Conclusions

An in situ study of structural development in amorphous poly(ethylene terephthalate) (PET) under uniaxial deformation above T_g (90 °C) was carried out using the synchrotron WAXD technique. The results showed several new insights into this subject. The load–strain curve can be divided into three zones (I, II, III), with each zone having its unique structure-property relationship. Zone I represents the development of the mesophase as a precursor for crystallization, which can be characterized by a constant load response with increasing strain. Zone II represents the strain-hardening region, which can be marked between the initial development of imperfect crystallites (with a loose triclinic unit cell) as well as the formation of stable crystalline structure and three-dimensional crystalline network. This zone contains several processes, which occur simultaneously including nucleation, growth, perfection and orientation. All these processes probably take place in the mesophase region. In Zone III, the formed crystal structure and the morphology become stable, which is characterized by a constant load–strain ratio. The crystal fraction is increased continuously with strain until the sample breaks. The molecular weight plays a particularly important role in

affecting the initiation and the span of these zones, and the ultimo strength.

Acknowledgements

The authors thank Toray Industry in Japan, the NSF Center for Advanced Engineering Fibers and Films at Clemson University (EEC-9731680), and NSF (DMR-0098104) for the financial support of this project. The authors also thank Mr Uchida from Toray for the synthesis of experimental PET samples.

References

[1] Bonart R. Kolloid-Z 1966;213:1.
[2] Yeh GSY, Geil PH. J Macromol Sci B 1967;1:235.
[3] Yeh GSY, Geil PH. J Macromol Sci B 1967;1:251.
[4] Lee S, Miyaji H, Geil PH. J Macromol Sci B 1983;22:489.
[5] Fakirov S. Handbook of thermoplastic polyesters: homopolymers, copolymers, blends and composites. London: Wiley; 2002.
[6] Liu J, Geil PH. J Macromol Sci B 1997;36:61.
[7] Asano T, Balta-Calleja FJ, Flores A, Tanigaki M, Mina MF, Sawatari C, Itagaki H, Takahashi H, Hatta I. Polymer 1999;40:6475.
[8] (a) Salem DR. Polymer 1992;33:3182. (b) Salem DR. Polymer 1992; 33:3189.
[9] Gorlier E, Haudin JM, Billion N. Polymer 2001;42:9541.
[10] LeBourvellec G, Monnerie L, Jarry JP. Polymer 1986;27:856.
[11] LeBourvellec G, Monnerie L, Jarry JP. Polymer 1987;28:1712.
[12] Spruiell JE, McCord DE, Beuerlein RA. Trans Soc Rheol 1972;16: 535.
[13] (a) Welsh GE, Blundell DJ, Windle AH. Macromolecules 1998;31: 7562. (b) Welsh GE, Blundell DJ, Windle AH. J Mater Sci 2000;35: 5225. (c) Blundell DJ, Mahendrasingam A, Martin C, Fuller W. J Mater Sci 2000;35:5057.
[14] (a) Mahendrasingam A, Blundell DJ, Martin C, Fuller W, MacKerron DH, Harvie JL, Oldman RJ, Riekel C. Polymer 2000;41:7803. (b) Blundell DJ, Mahendrasingam A, Martin C, Fuller W, MacKerron DH, Harvie JL, Oldman RJ, Riekel C. Polymer 2000;41:7793. (c) Mahendrasingam A, Martin C, Fuller W, Blundell DJ, Oldman RJ, MacKerron DH, Harvie JL, Riekel C. Polymer 2000;41:1217. (d) Blundell DJ, MacKerron DH, Fuller W, Mahendrasingam A, Martin C, Oldman RJ, Rule RJ, Riekel C. Polymer 1996;37:3303.
[15] Chaari F, Chaouche M, Doucet J. Polymer 2003;44:473.
[16] Ran S, Wang Z, Burger C, Chu B, Hsiao BS. Macromolecules 2002; 35:10102.
[17] Chu B, Hsiao BS. Chem Rev 2001;101(6):1727.
[18] Shimizu J. Sen'i-Gakkaishi 1985;38:243.
[19] Shimizu J, Kikutani T, Takaku A, Okui N. Sen'i-Gakkaishi 1981;37: T-135.
[20] Klug HP, Alexander LE. X-ray diffraction procedures. New York: Willey; 1954.
[21] Casey M. Polymer 1977;18:1219.
[22] Dalmage WJ, Geddes ALJ. Polym Sci 1958;31:499.
[23] Fraser RDB, MacRae TP, Millar A, Rowlands. J Appl Crystallogr 1976;9:81.
[24] Kawakami D, Ran S, Burger C, Fu B, Sics I, Chu B, Hsiao BS. Macromolecules 2003; in press.
[25] Glasstone S, Laider KJ, Eyring M. The theory of rate processes. New York: McGraw-Hill; 1941.
[26] Thompson AB. J Polym Sci 1959;34(127):741.
[27] Thompson AB. J Polym Sci 1959;37(131):313.
[28] George HH. Polym Engng Sci 1982;22(5):292.
[29] Doi M, Edwards SF. The theory of polymer dynamics. London: Oxford University Press; 1986.
[30] Somani RH, Hsiao BS, Nogales A, Srinivas S, Tsou AH, Sics I, Balta-Calleja FJ, Ezquerra TA. Macromolecules 2000;33(25):9385.
[31] Somani RH, Yang L, Hsiao BS, Agarwal P, Fruitwala H, Tsou AH. Macromolecules 2002;35(24):9096.
[32] Daubeny RD, Bunn CW, Brown CJ. Proc R Soc London Ser. A 1954; 226:531.
[33] Gupta KM, Motz H, Schultz JM. J Polym Sci, Polym Phys Ed 1983; 21:193.
[34] Goschel U, Deutscher K, Abez V. Polymer 1996;37(1):1.
[35] Huisman R, Heuvel HM. J Appl Polym Sci 1978;22:943.
[36] DeVries KL, Lloyd BA, Williams ML. J Appl Phys 1971;42:4644.
[37] Kaush HH. Rev Macromol Chem 1970;C4:243.